THE JOURNAL OF PHYSICAL CHEMISTRY C
A JOURNAL OF THE AMERICAN CHEMICAL SOCIETY

pubs.acs.org/JPCC

Article

One-Pot Separation of Semiconducting Single-Walled Carbon Nanotubes and Their Enantiomer Recognition Based on Self-Organized Supramolecular Riboflavin (Vitamin B2) Motifs

Wataru Ishimaru, Chaerin Kim, Fumiyuki Toshimitsu, Aleksandar Staykov, and Naotoshi Nakashima*

Cite This: https://doi.org/10.1021/acs.jpcc.2c00959

Read Online

ACCESS | Metrics & More | Article Recommendations | Supporting Information

ABSTRACT: The development of a facile method to sort semiconducting single-walled carbon nanotubes (s-SWCNTs) and their enantiomer recognition are still great challenges. We here describe a finding that a commercially available, safe, and cost-effective hydrophobic riboflavin analogue (riboflavin tetrabutyrate; **RTB**) efficiently sorts only s-SWCNTs by a one-pot method (bath-type sonication for 30 min followed by ultracentrifugation) and recognizes their enantiomers (left- and right-handed s-SWCNTs). The solubilization behavior of the SWCNTs strongly depends on the concentration of **RTB**; namely, with the decrease in the concentration of **RTB**, the s-SWCNT (*n*,*m*)-chiral selective sorting efficiency is enhanced. When using **RTB** = ∼0.4 mM (SWCNTs = 1 mg/3 mL toluene), two (*n*,*m*) chiralities of the s-SWCNTs with (*n*,*m*) = (8,6) and (8,7) were efficiently sorted. Furthermore, when using **RTB** = 0.5−1 mM, the SWCNT enantiomer recognition was observed. In addition, the X-ray photoelectron spectroscopic study revealed that the adsorbed **RTB** molecules on the s-SWCNTs were readily removed by simple rinsing with acetone to provide adsorbent-free pure s-SWCNTs. On the basis of the experimentally obtained data using Raman, photoluminescence, and visible−near-IR absorption spectroscopy techniques and computational density functional theory (DFT) approaches, we have revealed a possible mechanism for this unique s-SWCNT selective sorting and their enantiomer recognition. The supramolecular orientation of **RTB** into the helical superlattice with its own chirality provides a mechanism for chirality recognition. The study demonstrates one-pot sorting of s-SWCNTs and their enantiomer recognition using a cost-effective, safe molecule. Such a study is important for s-SWCNT separation science and its application in nanoscience and engineering areas.

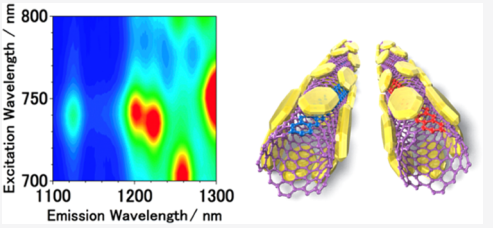

INTRODUCTION

Single-walled carbon nanotubes (SWCNTs) are unique one-dimensional structured nanomaterials that possess remarkable electronic, mechanical, thermal, and photonic/optical properties along with high chemical stability.[1−6] Their characteristic quantum-confined structures derived from chiral indices, denoted (*n*,*m*)SWCNTs, are important for a deep understanding of their fundamental intrinsic properties.[6−14] The synthesized SWCNTs are mixtures of semiconducting (s-) and metallic (met-)SWCNTs, and their properties and application areas are quite different. Thus, the separation/purification of the s-SWCNTs on the basis of their chiralities is still one of the most important issues in the science and applications of carbon nanotubes. Many approaches have already been reported regarding s-SWCNT sorting[2−41] from as-synthesized SWCNTs, which are a mixture of s-SWCNTs and met-SWCNTs, while many of them are complex in the separation. For one-pot easy separation, we need to design a suitable solubilizer by an organic/polymer synthesis method. Thus, the finding of an easy s-SWCNT separation technique is still a great challenge and highly important.

In this study, we describe that a commercially available, safe and cost-effective hydrophobic riboflavin analogue (riboflavin tetrabutyrate; **RTB**, Figure 1) efficiently sorts only s-SWCNTs by a one-pot method (bath-type sonication for 30 min followed

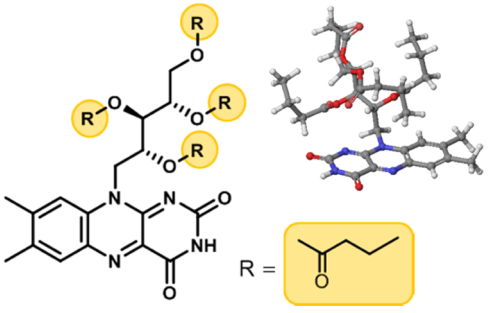

Figure 1. Chemical structure of **RTB**.

Received: February 9, 2022
Revised: May 18, 2022

by ultracentrifugation) and recognizes their enantiomers (left- and right-handed s-SWCNTs). Using a commercially available, safe, and cost-effective adsorbent that extracts only s-SWCNTs solely by sonication is a great benefit to s-SWCNT separation science.

The separated s-SWCNTs are composed of right- and left-handed SWCNT enantiomers, but the study on such enantiomer separation/recognition has been limited. Papadimitrakopoulos et al. reported that flavin mononucleotides (FMNs) recognized semiconducting left-handed and right-handed s-SWCNTs based on their helical assemblies.[42] Wei et al.[43] reported that a flavin mononucleotide (FMN), a chiral compound, recognized right- and left-handed SWCNTs when the SWCNTs were solubilized in water. Namely, using a gel chromatography technique, they found that the photoluminescence (PL) spectra of the solubilized (6,5)SWCNTs provided two different spots from the right- and left-handed SWCNTs due to the different microenvironments between the FMN and right- and left-handed SWCNTs. We reported the separation of right- and left-handed s-SWCNTs from as-produced SWCNTs using designed copolymers composed of polyfluorene (PFO) and chiral bulky moieties $(9,9\text{-dioctylfluorene-2,7-diyl})_x$((R)- or (S)-2,2′-dimethoxy-1,1′-binaphthalen-6,6-diyl)$_y$, where x and y are the copolymer composition ratios using a simple one-pot sonication method, in which the copolymers extracted either the right- or left-handed s-SWCNT enantiomers with (6,5)- and (7,5)-enriched chiralities.[44]

Zheng et al.[45] reported the use of intrinsically chiral single-stranded DNA (ssDNA) to achieve simultaneous handedness and chirality control for SWCNTs using two polymer-based aqueous two-phase systems, in which they screened more than 300 short ssDNA sequences with a palindromic symmetry, leading to the selection of more than 20 distinct SWCNT structures that have defined chirality and handedness of the SWCNTs. Jagota et al.[46] examined the physical basis of such selectivity using a coarse-grained model to compute the energetics of the ssDNA wrapped around an SWCNT and suggested that the difference by handedness of the SWCNT requires a spontaneous twist of the ssDNA backbone. Wei et al.[47] reported separating single-chirality SWCNT enantiomers by column chromatography in combination with overloading the selective adsorption and stepwise elution using a mixed surfactant and carried out an excitonic band structure analysis by assigning all of the observed E_{ii} and E_{ij} (i_v–j_c) optical transitions in the circular dichroism spectra of the sorted SWCNTs. A high-yield and high-throughput single-chirality SWCNT enantiomer separation method using stepwise elution gel chromatography has been described by Kataura et al.[48] Recently, Flavel et al.[49] applied a two-stage aqueous two-phase extraction technique for SWCNTs with diameters of >1.1 nm and succeeded in the separation of the enantiomer-pure fractions of R-(14,6), L-(14,6), R-(16,3), R-(15,5), and R-(13,7) with diameters of ∼1.41 nm with a single-chirality purity of up to 80%. Recently, Xu et al.[50] reported an SWCNT handedness separation method using acid cleavable polyfluorenes all with R- or S-configuration.

There is strong solvent dependence on the SWCNT enantiomer recognition, especially toluene and xylene with low dielectric constants are suitable solvents for both the selective s-SWCNT sorting and SWCNT enantiomer recognition.[34,44] However, FMN and riboflavin (or vitamin B2) are not soluble in such solvents because they are hydrophilic molecules. Based on such a background, in this study, we selected a toluene-soluble flavin, *i.e.*, **RTB**, Figure 1, and examined its s-SWCNT/met-SWCNT separation and s-SWCNT enantiomer recognition ability. In this paper, we describe (i) the finding that **RTB** individually sorts only s-SWCNTs from the mixture of the s-SWCNTs and met-SWCNTs, (ii) the unique PL splitting phenomenon from the (8,6)SWCNTs when the **RTB** concentration was very low, and (iii) a mechanism for the (8,6)SWCNT enantiomer recognition using **RTB**. Figure 2 depicts a schematic drawing of one-pot easy s-SWCNT sorting/recognition based on the self-assembled **RTB** on the SWCNT surfaces.

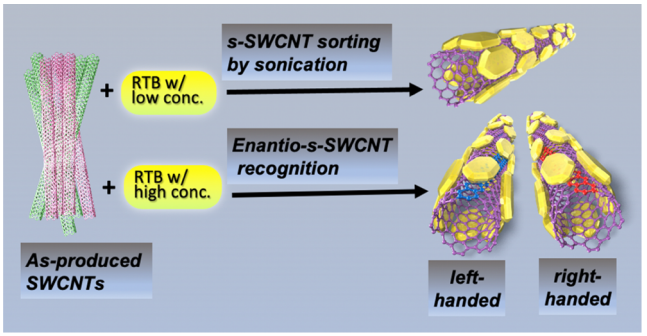

Figure 2. Schematic illustration of one-pot easy s-SWCNT sorting and SWCNT enantiomer recognition only by sonication using **RTB**.

METHODS

Materials, Sample Preparation, and Measurements. **RTB** (mp, 147.0−151.0 °C) was purchased from TCI Co., Ltd. and used as received. The SWCNTs (HiPco) were purchased from Carbon Nanotechnologies, Inc. and used as received. In this study, we prepared 17 different samples by changing the concentration of **RTB** in the range of 0.30−2.44 mM. The typical SWCNT solubilization/dispersion procedure[34,35] is as follows. The SWCNTs (1.0 mg) and **RTB** with a given concentration were sonicated in toluene (3.0 mL) for 1 h using a bath-type sonicator (Nano Premixer PR-1, THINKY Co., Ltd.), and the dispersion was centrifuged at 10,000*g* using a centrifuge (Himac CS150GXL instrument equipped with a swinging bucket rotor S55A, Hitachi High-Technologies Corporation) for 1 h; then, the supernatant (upper 80%) was separated to use for the measurements. The PL and visible−near-IR (vis−NIR) absorption spectra were recorded using a spectrofluorometer (Horiba-Jobin Yvon, SPEX Fluorolog-3-NIR) equipped with a liquid-nitrogen-cooled InGaAs near-IR detector and a spectrophotometer (JASCO, V-570), respectively. The excitation and emission wavelengths were in the ranges of 500−900 and 900−1300 nm, respectively. The Raman spectra were recorded using a Raman touch (Nanophoton Corporation) by excitation at 633 nm.

Removal of the Adsorbent. The typical **RTB** removal procedure is as follows. First, toluene was evaporated from the **RTB**-sorted s-SWCNT solution, and then, the residue was well rinsed with acetone and dried to measure the X-ray photoelectron spectroscopy (XPS) diagram.

Simulations. The molecular mechanic simulations were carried out using MacroModel (Infocom, version 8.6) with the OPLS-2005 force field and a dielectric constant value of 2.3, which is the same as that of toluene. Minimization on the calculations was carried out using the Polak−Ribiere conjugate gradient with a convergence threshold on a gradient of 0.05 kJ mol^{-1}. Default values were used for all other parameters.

https://doi.org/10.1021/acs.jpcc.2c00959
J. Phys. Chem. C XXXX, XXX, XXX−XXX

The first-principles calculations in the study were performed using the periodic, plane wave density functional theory implemented in the Vienna Ab initio Software Package (VASP).[32] Throughout the study, we have utilized the Perdew−Burke−Erzenhof (PBE) exchange−correlation functional using projector augmented wave pseudopotentials.[33] The electron energies were converged to 10^{-6} eV using Gaussian smearing with a Sigma of 0.1 eV. The calculations were performed with a 300 eV cutoff energy. Owing to the large cell size, the calculations were performed at γ points only. Relaxation was only performed for the atomic positions. Relaxation was performed until the forces converged to values below 0.03 eV $Å^{-2}$. Throughout this study, we have used graphical visualization package VESTA.[34]

RESULTS AND DISCUSSION

(*n*,*m*)-Chiral Selective Sorting of s-SWCNT and Their PL Behavior. SWCNT solubilization was carried out by sonication of **RTB** (0.30−2.44 mM) and HiPco-SWCNTs (1.0 mg) in toluene (3 mL) at 15 °C for 1 h using a bath-type sonicator (Nano Premixer PR-1) by rotating each sample at 500 rpm during sonication, which is very efficient for obtaining homogeneous SWCNT dispersion samples. Thereafter, ultracentrifugation at 10,000*g* for 1 h at rt was carried out, and then, each supernatant (top 80%) was collected.

Raman spectroscopy is a powerful technique to evaluate the selective sorting of s-SWCNTs from the mixtures of s-SWCNTs and met-SWCNTs. Typical Raman spectra of the pristine SWCNTs and solubilized SWCNTs using **RTB** = 0.78 mM are shown in Figure 3, in which it is evident that **RTB** solubilized

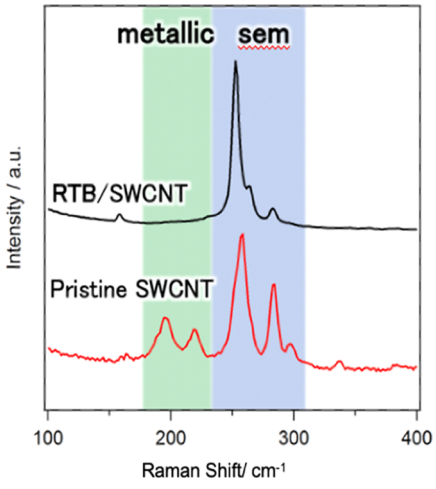

Figure 3. Raman spectra of pristine SWCNTs (red) and solubilized SWCNTs (supernatant; black) using **RTB** (0.78 mM) and SWCNTs (1 mg) in toluene (3 mL), by excitation at 633 nm.

only the s-SWCNTs because the peaks appeared only in the s-SWCNT wavelength range of 230−310 cm^{-1}, while no peaks appeared in the met-SWCNT range of 180−230 cm^{-1}.[33−35] Thus, s-SWCNT sorting selectivity is >99%. Almost the same selective s-SWCNT sorting behavior was obtained when using **RTB** = 0.41−2.44 mM. Figure 4 shows the typical vis−NIR absorption spectra of the solubilized SWCNTs. The absorption intensity is proportional to the amounts of solubilized nanotubes. We estimated the amount of the solubilized s-SWCNTs using **RTB**. When using 3 mL of **RTB** = 2.28 mM, the amount of the solubilized s-SWCNTs was 0.054 mg, which is comparable with those of flavin analogues reported previously.[34] When using **RTB** concentrations lower than 0.41 mM, SWCNT dissolution was not evident. The (*n*,*m*)SWCNT selective sorting showed **RTB** concentration dependence, as will be discussed later.

PL is a powerful method to evaluate the individual SWCNT solubilization performance because individually solubilized SWCNTs emit from their solutions. In this study, when using **RTB** = 0.30−0.36 mM in toluene (3 mL) containing 1 mg of SWCNTs, individual solubilization of the SWCNTs was not evident because we could not detect PL signals from the solutions due to the lack of a suitable amount of the dispersant. However, in the range of **RTB** = 0.41−2.44 mM, the SWCNTs were found to be individually solubilized. The two-dimensional PL (2D PL) mapping of the obtained **RTB**-dissolved SWCNT solutions (selected nine samples) is shown in Figure 5 (for the PL of all 17 samples, see the Supporting information, Figure S1). When using **RTB** = 2.44 mM, 18 PL spots from the solution with enriched chiralities of (*n*,*m*) = (8,6), (8,7), (9,5), and (10,5) together with (*n*,*m*) = (6,5), (7,5), (7,6), (8,4), (9,4), (9,7), (9,8), (10,2), (10,3), (10,6), (11,1), (11,4), (12,2), and (13,2) were noted. We also found that by decreasing the **RTB** concentrations, the number of PL spots from the solubilized (*n*,*m*) SWCNT decreased; namely, at **RTB** = 0.41 mM, only three PL spots of (*n*,*m*) = (8,6) and (8,7) (both enriched) and (9,7) were observed, indicating that the **TRB** concentration strongly affected the (*n*,*m*)-chiral selective SWCNT sorting.

Figure 6 shows the relative abundance (%) of the extracted (*n*,*m*)SWCNTs with 17-(*n*,*m*) different chiralities as a function of the **TRB** concentrations used for the SWCNT solubilization (for detail, see Table S1), in which each (*n*,*m*)SWCNT abundance was determined based on the quantum yield-corrected (*n*,*m*)SWCNT PL intensities.[51] Data for all of the samples are plotted in Figure 6a. We then classified them into three categories, as shown in Figure 6b−d. The **RTB** concentrations were not sufficient for the provided 12 (*n*,*m*)SWCNT chiralities, as shown in Figure 6b. In sharp contrast, the SWCNTs with chiralities of (*n*,*m*) = (8,6) and (8,7) showed strong **RTB** concentration dependence; namely, at the lower concentration below **RTB** = 0.5 mM, the abundance (%) of (8,6) and (8,7)SWCNTs significantly increased. Such a trend was not very significant for the (9,7)SWCNTs, while it still existed when **RTB** = 0.4 mM. For the (9,5) and (11,6)-SWCNTs, with a decrease in the concentration of **RTB**, their abundance somewhat increased, while at the **RTB** concentration lower than 0.45 mM, it decreased, and at **RTB** = 0.4 mM, it became almost zero (Figure 6d). We further discuss the observed unique **RTB** concentration-dependent (*n*,*m*)SWCNT solubilization behavior. The diameter range and chiral angles of all of the detected (*n*,*m*)SWCNTs, except for the (8,6), (8,7), and (9,7)SWCNTs, are 0.75−1.15 nm, which is very widely dispersed, and 7.05−28.05° (also widely distributed), respectively. In sharp contrast, the diameter range and chiral angle range of the (8,6), (8,7), and (9,7) (plotted as red-colored lines) of the SWCNTs are 0.95−1.09 nm and 25.28−27.80° (very narrow distribution), respectively. The diameter of the (9,5)-SWCNTs is 0.96 nm, which is between 0.95 and 1.09 nm, while their chiral angle is 20.63°, which is outside the range of 25.28−27.80°. The diameter of the (11,6)SWCNTs is 1.17 nm, which is not in the range of 0.95−1.09 nm, and its chiral angle is 20.36°, which is outside the range of 25.28−27.80°. We demonstrate that all of the results indicate that the **RTB** molecules recognize the differences in both the diameters and chiral angles of the

https://doi.org/10.1021/acs.jpcc.2c00959
J. Phys. Chem. C XXXX, XXX, XXX−XXX

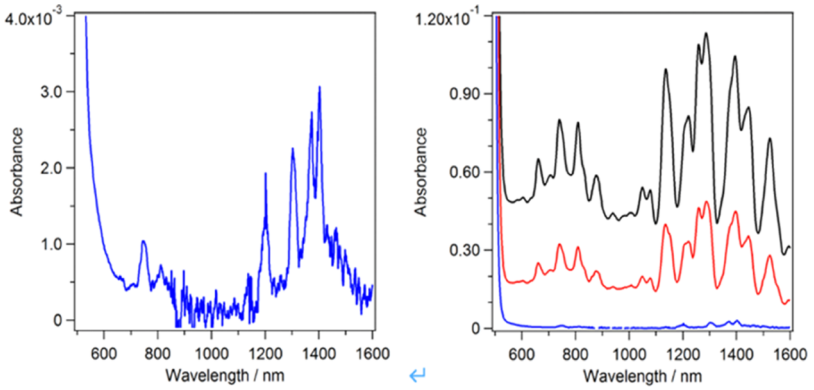

Figure 4. Vis−NIR absorption spectra of the solubilized SWCNTs (supernatant) using **RTB** = 0.41 mM (left column and right column, blue color), 1.22 mM (right column, red color), and 1.52 mM (right column, black color) in toluene (3 mL). The sonication procedure was carried out in the presence of the SWCNTs (1 mg). The optical path length was 1.0 cm.

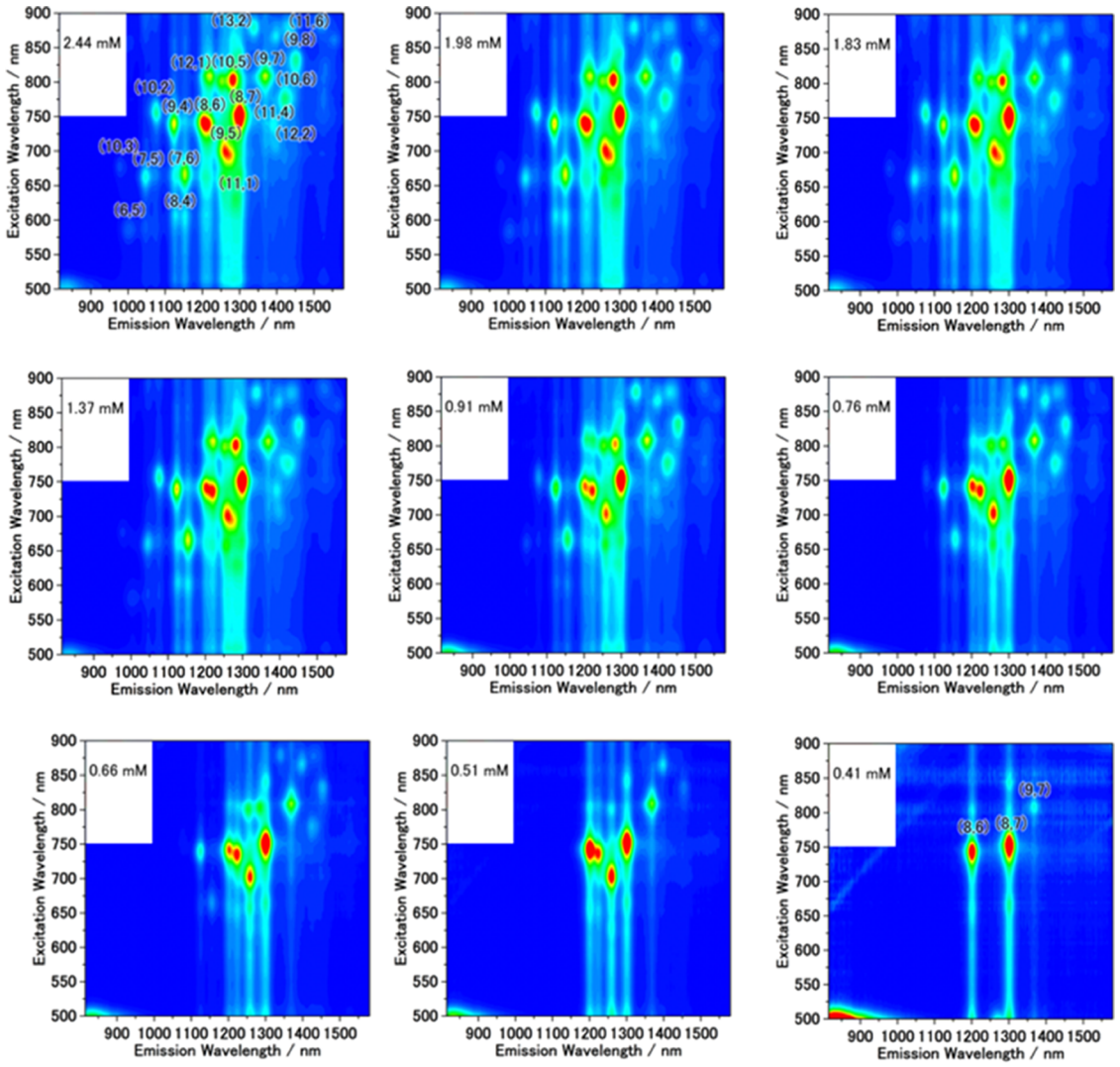

Figure 5. 2D PL mapping images of nine selected SWCNT solutions (supernatant) in toluene using **RTB**. The **RTB** concentrations for the solubilization are provided in the figures. The sonication procedure was carried out in the presence of SWCNTs (1 mg). For the detailed preparation procedure, see Methods section.

SWCNTs with (n,m) = (8,6), (8,7), and (9,7) from those of the other (n,m)SWCNTs.

Splitting of PL and NIR Absorption Bands and SWCNT Enantiomer Recognition. We now focus on the PL splitting of the solubilized SWNCTs obtained by **RTB** of different concentrations. As shown in Figure 5, the PL from the (8,6)SWCNTs is observed at **RTB** = 1.52−0.51 mM concentrations. To further clarify, the PL from the (8,6)-

https://doi.org/10.1021/acs.jpcc.2c00959
J. Phys. Chem. C XXXX, XXX, XXX−XXX

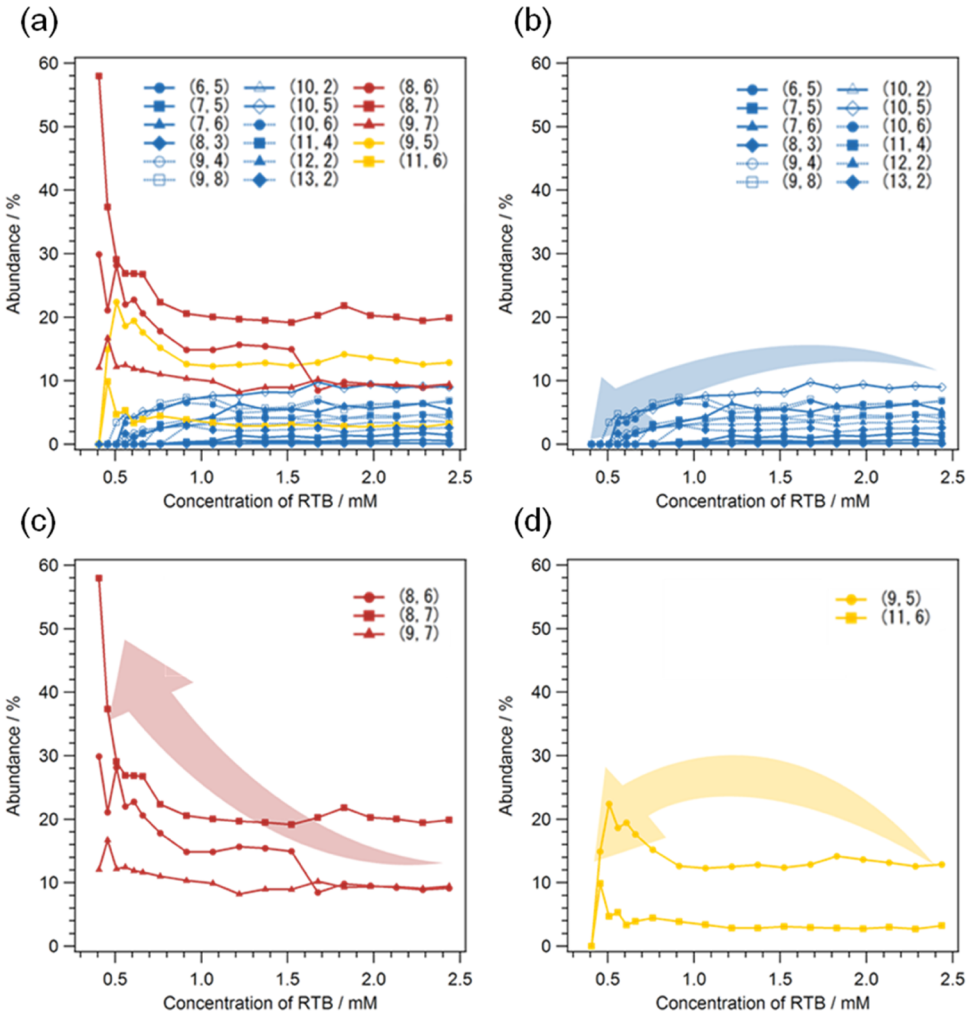

Figure 6. Relative abundances of the dissolved (*n*,*m*)SWCNTs (supernatant) as a function of the **RTB** concentration for solubilization. Plotted (*n*,*m*)chiralities are provided in columns (a−d). The sonication procedure was carried out in toluene (3 mL) in the presence of SWCNTs (1 mg).

SWCNTs is enlarged in Figure 7, in which the PL clearly splits into two spots, as shown in Figure 7b,c. More interestingly, at **RTB** = 0.41 mM, one of the split PL spots at around 1200 nm disappeared, and as a result, we see only one spot, as shown in Figure 7d. The obtained result agrees well with the Raman data shown in Figure 8, in which we only detect one peak at 252 cm^{-1} from the solubilized solution that is ascribable to the (8,6)SWCNTs, which is detectable when excited at 633 nm. Considering the **RTB**-induced transition peak shift based on the report by Wei et al,[43] we consider that the spot at ∼1220 nm would be ascribed to the enriched left-handed (8,6)SWCNTs, and the ∼1200 nm band would be ascribed to the right-handed (8,6)SWCNTs. The results indicated that **RTB** has the ability of SWCNT enantiomer recognition and sorting by choosing the suitable **RTB** concentrations.

The NIR spectra of 17 **RTB**-dissolved s-SWCNTs are shown in the Supporting Information, Figures S2 and S3, in which the absorbance of the extracted semiconducting SWCNTs was 0.15−0.002. When using **RTB** = 2.44 mM, it was 0.15, which was ∼2.1 times larger than that using PFO.[52] However, PFOs[52] have no ability to recognize left- and right-handed SWCNTs.

Band splitting was also observed in the NIR absorption spectra. A typical result is shown in Figure 9; at **RTB** = 2.44 mM, we observed one broad peak at ∼1212 nm, and similar results were obtained when using **RTB** = 2.44−1.67 mM. In sharp

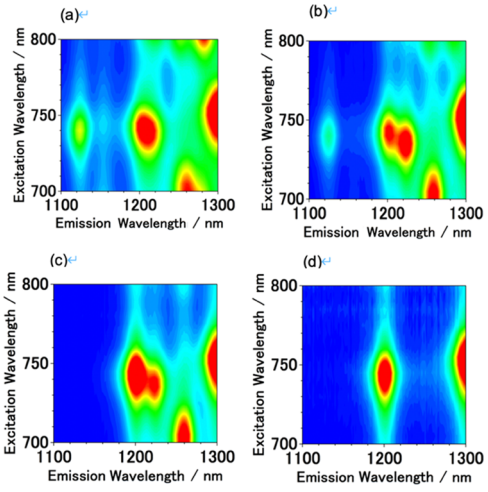

Figure 7. 2D PL mapping images focused on (8,6)SWCNTs solubilized using **RTB**. The **RTB** concentrations used in the solubilization procedures are (a) 1.83 mM, (b) 0.66 mM, (c) 0.51 mM, and (d) 0.41 mM in toluene (3 mL) containing SWCNTs (1 mg) for sonication.

contrast, when using **RTB** concentrations lower than 1.52 mM, the absorption bands became broad, and then, at **RTB** = 0.61

https://doi.org/10.1021/acs.jpcc.2c00959
J. Phys. Chem. C XXXX, XXX, XXX−XXX

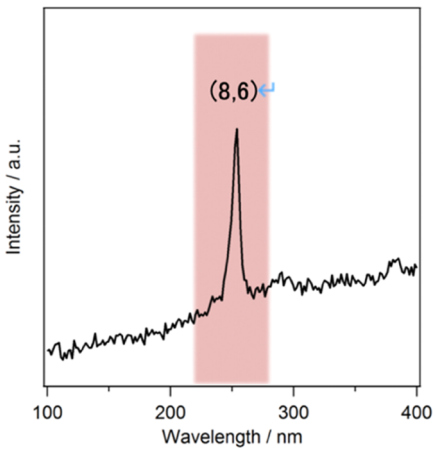

Figure 8. Raman spectrum (**RBM** region) of the dissolved SWCNTs in toluene (3 mL) using SWCNTs (1 g) and **RTB** = 0.41 for sonication; excitation, 633 nm.

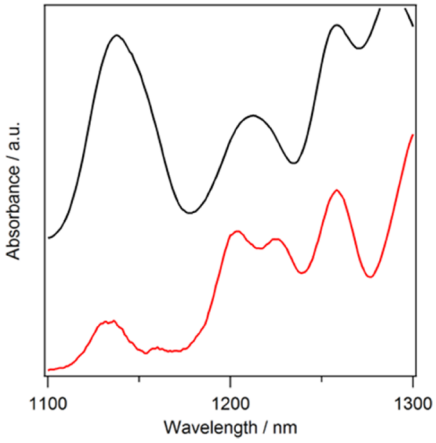

Figure 9. NIR absorption spectra of **RTB**-dissolved SWCNTs in toluene (3 mL) using SWCNTs (1 g) and **RTB** = 2.44 mM (black line) or **RTB** = 0.61 mM (red line).

mM, it clearly splits into two peaks (peak top wavelengths = ~1204 and ~1225 nm). A similar result was obtained when using **RTB** = 0.41 mM. Such obtained NIR absorption results agreed well with the obtained PL and Raman results. In the study, **RTB** is a chiral compound since the used riboflavin is (-)riboflavin with a specific rotation of $[\alpha]$ (20 °C) = −30° cm^2/g. FMN has been reported to recognize right- and left-handed SWCNTs when FMN was used to solubilize the SWCNTs in water;[42] however, in that study, selective s-SWCNT sorting was not possible because the solubilization procedure was carried out in water, and the enantiomer (8,6)SWCNT and (11,−5)SWCNT separations were carried out using a gel column chromatography technique, which is not simple.

We have measured CD spectra of the **RTB**/SWCNT toluene solution, and the result is shown in Figure S4, in which no CD signal was detected, suggesting that the separation of s-SWCNT enantiomer using **RTB** was difficult, which suggested that the **RTB** solubilized both right-handed and left-handed s-SWCNTs, and enantiomer excess in the sorting process was not sufficient to separate the right-handed and left-handed s-SWCNTs. Such behavior was different from cited paper #44, in which we have reported a one-pot s-SWCNT enantiomer separation using synthesized fluorene-binaphthol chiral copolymers. The detection of the splitting of NIR-PL and NIR absorption spectra shown in Figures 7 and 9, respectively, suggested that the **RTB** molecules have left-/right-handedness-dependent interactions since **RTB** is a chiral compound. Such behavior agrees with the previously reported result.[43]

Removal of Solubilizers. As we described in the previous paper,[34] the removal of the adsorbents from the separated s-SWCNTs provided adsorbent-free s-SWCNTs. Such an event is highly important because the remaining adsorbed solubilizer often decreases the intrinsic property of the s-SWCNTs in many application areas. In this study, the removal of the used solubilizer was very simple and easy; namely, only rinsing with acetone was enough, as described in the Methods section. The removal was confirmed by X-ray photoelectron spectroscopy (XPS) analyses, and the result is shown in Figure 10a, in which

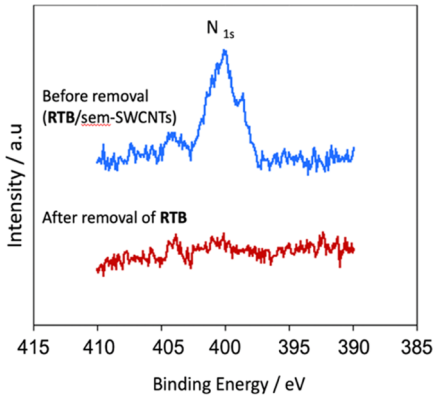

Figure 10. N 1s narrow-scan XPS spectra of the separated s-SWCNTs/**RTB** before (blue line) and after (red line) the **RTB** removal procedure.

the N 1s narrow-scan XPS spectrum of the separated s-SWCNTs by **RTB** shows no N 1s band (red line in the figure). Before the removal treatment, we clearly observed the N 1s band (blue line in the figure) at around the 400 eV region. A schematic drawing of this **RTB** removal is shown in Figure 10b. The wide-scan XPS spectra of the samples before and after the removal treatment are shown in Figure S5.

Computer Simulations. In a recent study, we have elucidated using density functional theory (DFT) methods the formation of the helical supramolecular structure of a flavin−Cu^{2+} supramolecular complex on the surface of the SWCNT (8,6)[35] (we also carried out molecular mechanics simulations; for the results, see the Supporting Information for the Simulations section, which includes Figure S6). We used DFT simulations to estimate the interaction of the chiral helical structure of **RTB** with the left- and right-handed CNT (8,6).[53−55] The results of the geometry optimization are summarized in Figure 11. We should mention that the chiral molecular arrangement of **RTB** in a helical superstructure represents close packing of **RTB** on the surface and corresponds to the highest possible density of **RTB** on the tube surface. Thus, it is worth investigating the interaction between the supramolecular helix and the right-and left-handed SWCNTs. The helical supramolecular structure depends on the molecular structure of the monomers and is shown in Figure 12. The **RTB** molecules are linked using hydrogen bonds, which determine the orientation and the pattern of the aromatic rings on the tube's surface. This pattern is different for the right- and left-handed SWCNTs, and it determines the strength of the $\pi-\pi$ stacking interaction between the **RTB** helix and the SWCNT.

https://doi.org/10.1021/acs.jpcc.2c00959
J. Phys. Chem. C XXXX, XXX, XXX−XXX

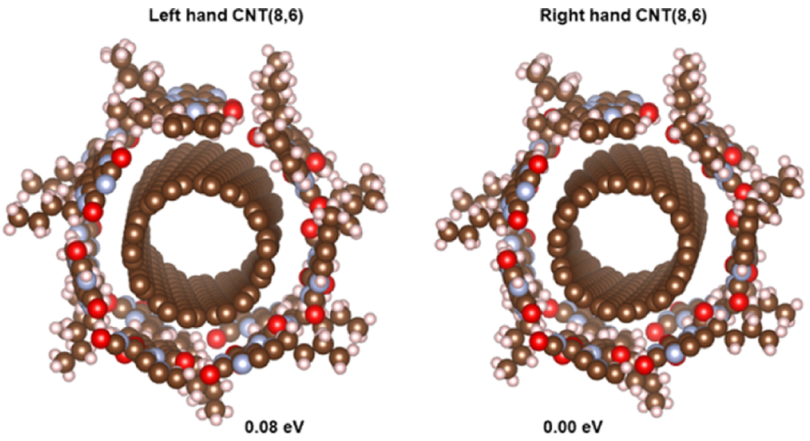

Figure 11. DFT-investigated models of left- and right-handed SWCNTs (8,6) with formation of **RTB** helical structures.

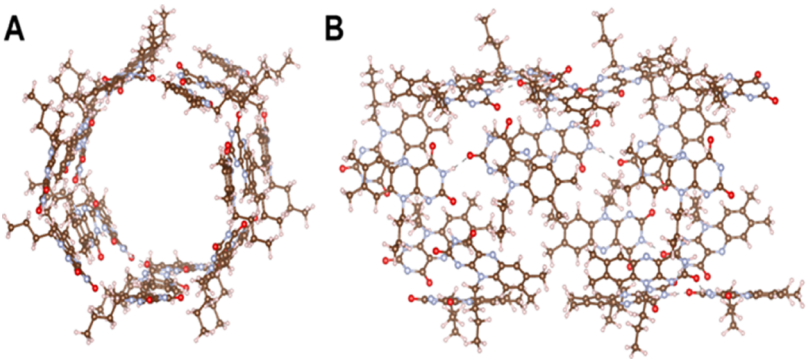

Figure 12. Model of the **RTB** supramolecular helix obtained by the DFT calculations. A, face view; B, side view.

The relative binding energy is shown in Figure 12, and it is 0.08 eV higher for the left-handed SWCNT (8,6). Thus, we can conclude that the **RTB** helix interacts stronger with the right-handed SWCNT (8,6).

On the basis of all of the obtained results, we now provide a possible **RTB** adsorption behavior scenario that would explain the (8,6)SWCNT enantiomer recognition that appeared at the very low **RTB** concentrations. At the higher **RTB** concentrations, such as **RTB** = 2.44 mM, the **RTB** molecules interact with the SWCNTs with many different (*n*,*m*) chiralities, resulting in their dissolution in the solvent because many PL spots are observed from the solution (see Figure 5a). Namely, for many (*m*,*n*)SWCNTs, almost no specific assembled **RTB** adsorption onto the SWCNTs at the higher **RTB** concentrations (RTB > 1.83 mM) is seen; meanwhile, for the (8,6)SWCNTs, we see a somewhat left-handed recognition. It is reasonable to consider that the excess amounts of **RTB** against the SWCNTs lack a selective recognition of the right- and left-handed chirality of the SWCNTs. In the concentration range of **RTB** = 1.52−0.51 mM, PL splitting of the (8,6)SWCNTs is observed, in which the **RTB** molecules can clearly recognize the enantiomers of the right- and left-handed (8,6)SWCNTs with a specific manner due to the suitable weight ratios of the **RTB** and SWCNTs, resulting in their PL splitting. Finally, at **RTB** = 0.41 mM, the **RTB** recognizes and solubilizes only the right-handed (8,6)SWCNTs.

■ CONCLUSIONS

In this study, we examined the one-pot selective dissolution of the SWCNTs using hydrophobic riboflavin (**RTB**) with different concentrations and revealed selective (*n*,*m*)-s-SWCNT sorting by simply changing the **RTB** concentrations. Namely, the (*n*,*m*) selectivity was higher when using lower **RTB** concentrations, and at **RTB** = 0.41 mM (SWCNTs = 1 mg in 3 mL of toluene), only two chiralities of (8,6) and (8,7)SWCNTs were enriched together with a small amount of the (9,7)-SWCNTs. The **RTB** molecules recognize the differences of both the diameters and chiral angles of the SWCNTs when solubilization occurs by sonication. Furthermore, at **RTB** = 0.5−1 mM, it showed SWCNT enantiomer recognition because the PL splitting that is derived from the right- and left-handed (8,6)SWCNTs was observed. On the basis of the presented experimental and computational DFT calculations, such unique SWCNT selective sorting and its enantiomer recognition behavior are due to a specific/suitable concentration-dependent **RTB** adsorption by an assembled structure (Figures 11 and 12). The major recognition behavior is due to the specific interaction between the **RTB** supramolecular helix and the right- and left-handed SWCNTs. The chirality of the tube controls the strength of the $\pi-\pi$ stacking interaction. Thus, the chirality of the supramolecular helix interacts with the chirality of the SWCNTs and results in chirality recognition.

Finally, we would like to emphasize that a commercially available cost-effective hydrophobic flavin analogue (**RTB**) efficiently sorts the s-SWCNTs only in one pot (bath-type sonication for 30 min) and recognizes their enantiomers. This study provides a promising method to develop a simple way for highly selective s-SWCNT sorting with the desired (*n*,*m*)-chirality, which is useful in both fundamental studies and applications of SWCNTs using their unique (*n*,*m*)-dependent optical and electronic properties. Furthermore, the study would

https://doi.org/10.1021/acs.jpcc.2c00959
J. Phys. Chem. C XXXX, XXX, XXX−XXX

be of importance in view of the practical applications of s-SWCNTs in the semiconductor industry.

■ ASSOCIATED CONTENT

Supporting Information

The Supporting Information is available free of charge at https://pubs.acs.org/doi/10.1021/acs.jpcc.2c00959.

2D PL mapping images of dissolved 17 SWCNTs in toluene using **RTB**, vis−NIR absorption spectra of the solubilized SWCNTs in toluene at the provided **RTB** concentration, wide-scan XPS diagrams of the sorted s-SWCNTs before and after the **RTB** removal procedure, abundance of chiralities at given **RTB** concentrations, and all authors of references #6 and #27 (PDF)

■ AUTHOR INFORMATION

Corresponding Author

Naotoshi Nakashima − *International Institute for Carbon-Neutral Energy Research (WPI-I2CNER), Kyushu University, Fukuoka 819-0395, Japan;* orcid.org/0000-0002-7890-4531; Email: nakashima.naotoshi.614@m.kyushu-u.ac.jp

Authors

Wataru Ishimaru − *Department of Applied Chemistry, Kyushu University, Fukuoka 819-0395, Japan*

Chaerin Kim − *International Institute for Carbon-Neutral Energy Research (WPI-I2CNER), Kyushu University, Fukuoka 819-0395, Japan*

Fumiyuki Toshimitsu − *International Institute for Carbon-Neutral Energy Research (WPI-I2CNER), Kyushu University, Fukuoka 819-0395, Japan;* orcid.org/0000-0001-6642-9043

Aleksandar Staykov − *International Institute for Carbon-Neutral Energy Research (WPI-I2CNER), Kyushu University, Fukuoka 819-0395, Japan;* orcid.org/0000-0003-2572-1317

Complete contact information is available at: https://pubs.acs.org/10.1021/acs.jpcc.2c00959

Author Contributions

The manuscript was written through the contribution of all authors. All authors have given approval to the final version of the manuscript.

Notes

The authors declare no competing financial interest.

■ ACKNOWLEDGMENTS

This study was supported by JSPS KAKENHI Grant Number JP16H02083 from the Ministry of Education, Culture, Sports, Science, and Technology (MEXT), Japan and the Nanotechnology Platform Program (Molecule and Material Synthesis) of the Ministry of Education, Culture, Sports, Science, and Technology (MEXT), Japan, Grant Number JPMXP09 S21KU0046.

■ REFERENCES

(1) Iijima, S.; Ichihashi, T. Single-Shell Carbon Nanotubes of 1-nm Diameter. *Nature* **1993**, *363*, 603−605.

(2) Ouyang, M.; Huang, J.-L.; Lieber, C. M. Fundamental Electronic Properties and Applications of Single-Walled Carbon Nanotubes. *Acc. Chem. Res.* **2002**, *35*, 1018−1025.

(3) O'Connell, M. J.; Bachilo, S. M.; Huffman, C. B.; Moore, V. C.; Strano, M. S.; Haroz, E. H.; Rialon, K. L.; Boul, P. J.; Noon, W. H.; Kittrell, C.; Ma, J.; Hauge, R. H.; Weisman, R. B.; Smalley, R. E. Band Gap Fluorescence from Individual Single-Walled Carbon Nanotubes. *Science* **2002**, *297*, 593−596.

(4) Jorio, A.; Dresselhaus, M. S.; Dresselhaus, D. *Carbon Nanotubes-Topics in Applies Physicss 111*; Springer-Verlag: Heideeelberg, Germany, 2008.

(5) Yang, F.; Wang, M.; Zhang, D.; Yang, J.; Zheng, M.; Li, Y. Chirality Pure Carbon Nanotubes: Growth, Sorting, and Characterization. *Chem. Rev.* **2020**, *120*, 2693−2758.

(6) Rao, R.; Pint, C. L.; Islam, A. E.; Weatherup, R. S.; Hofmann, S.; Meshot, E. R.; Wu, F.; Zhou, C.; Dee, N.; Amama, P. B.; et al. Carbon nanotubes and related nanomaterials: Critical Advances and Challenges for Synthesis Toward Mainstream Commercial Applications. *ACS Nano* **2018**, *12*, 11756−11784.

(7) Hu, L.; Hecht, D. S.; Grüner, G. Carbon Nanotube Thin Films: Fabrication, Properties, and Applications. *Chem. Rev.* **2010**, *110*, 5790−5844.

(8) Lin, C.-W.; Yang, H.; Sanchez, R. S.; Mao, W.; Pang, L.; Beckingham, K. M.; Bast, R. C.; Weisman, R. B. In Vivo Optical Detection and Spectral Triangulation of Carbon Nanotubes. *ACS Appl. Mater. Interfaces* **2017**, *9*, 41680−41690.

(9) Lefebvre, J.; Ding, J.; Li, Z.; Finnie, P.; Lopinski, G.; Malenfant, P. R. L. High-Purity Semiconducting Single-Walled Carbon Nanotubes: A Key Enabling Material in Emerging Electronics. *Acc. Chem. Res.* **2017**, *50*, 2479−2486.

(10) Song, J.; How, P. X.; Chen, K. L.; Wang, B.-W.; Sun, D. M.; Tang, D. M.; Jin, Q.; Zhang, D. D.; Du, J. H.; Tai, K. P.; Tan, J.; Kauppinen, E. I.; Cheng, H. M. Ultrahigh-performance Transparent Conductive Films of Carbon-welded Isolated Single-wall Carbon Nanotubes. *Sci. Adv.* **2018**, *4*, 9262.

(11) *Nanocarbons for Energy Conversion-Supramolecular Approaches*; Nakashima, N., Ed.; Springer, 2018; pp 1−564.

(12) Qiu, S.; Wu, K.; Gao, B.; Li, L.; Jin, H.; Li, Q. Solution-Processing of High-Purity Semiconducting Single-Walled Carbon Nanotubes for Electronics Devices. *Adv. Mater.* **2019**, *31*, No. 1800750.

(13) Yang, J.; Ganesan, P.; Ishihara, A.; Nakashima, N. Carbon Nanotube-based Non-precious Metal Electrode Catalysts for Fuel Cells, Water Splitting and Zinc-air Batteries. *ChemCatChem* **2019**, *11*, 5929−5944.

(14) Gaviria Rojas, W. A.; Hersam, M. C. Chirality-Enriched Carbon Nanotubes for Next-Generation Computing. *Adv. Mater.* **2020**, *32*, No. 1905654.

(15) Arnold, M. S.; Green, A.; Hulvat, J. F.; Stupp, S. I.; Hersam, M. C. Sorting Carbon Nanotubes by Electronic Structure using Density Differentiation. *Nat. Nanotechnol.* **2006**, *1*, 60−65.

(16) Peng, X.; Komatsu, N.; Bhattacharya, S.; Shimawaki, T.; Aonuma, S.; Kimura, T.; Osuka, A. Optically Active Single-walled Carbon Nanotubes. *Nat. Nanotechnol.* **2007**, *2*, 361−365.

(17) Tu, X.; Manohar, S.; Jagota, A.; Zheng, M. DNA Sequence Motifs for Structure-specific Recognition and Separation of Carbon Nanotubes. *Nature* **2009**, *460*, 250−253.

(18) Green, A. A.; Duch, M. C.; Hersam, M. C. Isolation of Single-Walled Carbon Nanotube Enantiomers by Density Differentiation. *Nano Res.* **2009**, *2*, 69−77.

(19) Ghosh, S.; Bachilo, S. M.; Weisman, R. B. Advanced Sorting of Single-walled Carbon Nanotubes by Nonlinear Density-gradient Ultracentrifugation. *Nat Nanotechnol.* **2010**, *5*, 443−450.

(20) Lee, H. W.; Yoon, Y.; Park, S.; Oh, J. H.; Hong, S.; Liyanage, L. S.; Wang, H.; Morishita, S.; Patil, N.; Park, Y. J.; et al. Selective Dispersion of High Purity Semiconducting Single-walled Carbon Nanotubes with Regioregular Poly(3-alkylthiophene)s. *Nat. Commun.* **2011**, *2*, No. 541.

(21) Ozawa, H.; Fujigaya, T.; Niidome, Y.; Hotta, N.; Fujiki, M.; Nakashima, N. Rational Concept to Recognize/extract Single-walled Carbon Nanotubes with a Specific Chirality. *J. Am. Chem. Soc.* **2011**, *133*, 2651−2657.

(22) Miyata, Y.; Shiozawa, K.; Asada, Y.; Ohno, Y.; Kitaura, R.; Mizutani, T.; Shinohara, H. Length-sorted Semiconducting Carbon

Nanotubes for High-mobility Thin film Transistors. *Nano Res.* **2011**, *4*, 963−970.
(23) Hirano, A.; Tanaka, T.; Kataura, H. Thermodynamic Determination of the Metal/Semiconductor Separation of Carbon Nanotubes Using Hydrogels. *ACS Nano* **2012**, *6*, 10195−10205.
(24) Khripin, C. Y.; Fagan, J.; Zheng, M. Spontaneous Partition of Carbon Nanotubes in Polymer-modified Aqueous Phases. *J. Am. Chem. Soc.* **2013**, *135*, 6822−6825.
(25) Tulevski, G. S.; Franklin, A.; Afzali, A. High Purity Isolation and Quantification of Semiconducting Carbon Nanotubes via Column Chromatography. *ACS Nano* **2013**, *7*, 2971−2976.
(26) Gomulya, W.; Costanzo, G. D.; Figueiredo de Carvalho, E. J.; Bisri, S. Z.; Derenskyi, V.; Fritsch, M.; Fröhlich, N.; Allard, S.; Gordiichuk, P.; Herrmann, A.; et al. Semiconducting Single-walled Carbon Nanotubes on Demand by Polymer Wrapping. *Adv. Mater.* **2013**, *25*, 2948−2956.
(27) Toshimitsu, F.; Nakashima, N. Semiconducting Single-walled Carbon Nanotubes Sorting with a Removable Solubilizer Based on Dynamic Supramolecular Coordination Chemistry. *Nat. Commun.* **2014**, *5*, No. 5041.
(28) Ao, G.; Khripin, C. Y.; Zheng, M. DNA-controlled Partition of Carbon Nanotubes in Polymer AqueousTwo-phase Systems. *J. Am. Chem. Soc.* **2014**, *136*, 10383−10392.
(29) Liu, H.; Tanaka, T.; Kataura, H. Optical Isomer Separation of Single-Chirality Carbon Nanotubes Using Gel Column Chromatography. *Nano Lett.* **2014**, *14*, 6237−6243.
(30) Pochorovski, I.; Wang, H.; Feldblyum, J. I.; Zhang, X.; Antaris, A. L.; Bau, Z. H-Bonded Supramolecular Polymer for the Selective Dispersion and Subsequent Release of Large-Diameter Semiconducting Single-Walled Carbon Nanotubes. *J. Am. Chem. Soc.* **2015**, *137*, 4328−4331.
(31) Tanaka, T.; Urabe, Y.; Hirakawa, T.; Kataura, H. Simultaneous Chirality and Enantiomer Separation of MetallicSingle-wall Carbon Nanotubes by Gel column Chromatography. *Anal. Chem.* **2015**, *87*, 9467−9472.
(32) Reis, W. G.; Weitz, R. T.; Kettner, M.; Kraus, A.; Schwab, M. G.; Tomović, Ž.; Krupke, R.; Mikhael, J. Highly Efficient and Scalable Separation of Semiconducting Carbon Nanotubes via Weak Field Centrifugation. *Sci. Rep.* **2016**, *6*, No. 26259.
(33) Toshimitsu, F.; Nakashima, N. Facile Isolation of Adsorbent-Free Long and Highly-Pure Chirality-Selected Semiconducting Single-Walled Carbon Nanotubes Using A Hydrogen-bonding Supramolecular Polymer. *Sci. Rep.* **2015**, *5*, No. 18066.
(34) Nakashima, N.; Fukuzawa, M.; Nishimura, K.; Fujigaya, T.; Kato, Y.; Staykov, A. Supramolecular Chemistry-based One-pot High-efficient Separation of Solubilizer-free Pure Semiconducting Single-walled Carbon Nanotubes: Molecular strategy and Mechanism. *J. Am. Chem. Soc.* **2020**, *142*, 11847−11856.
(35) Staykov, A.; Hashimoto, W.; Toshimitsu, F.; Nakashima, N. A Flavin-Cu2+ Supramolecular Complex for Highly Selective Sorting of Semiconducting Single-walled Carbon Nanotubes with Specific Chiralities. *Chem. Commun.* **2020**, *56*, 12415−12418.
(36) Yomogida, Y.; Tanaka, T.; Tsuzuki, M.; Wei, X.; Kataura, H. Automatic Sorting of Single-Chirality Single-Wall Carbon Nanotubes Using Hydrophobic Cholates: Implications for Multicolor Near-Infrared Optical Technologies. *ACS Appl. Nano Mater.* **2020**, *3*, 11289−11297.
(37) Yang, X.; Liu, T.; Li, R.; Yang, X.; Lyu, M.; Fang, L.; Zhang, L.; Wang, K.; Zhu, A.; Zhang, L.; Qiu, C.; Zhang, Y.-Z.; Wang, X.; Peng, L.-M.; Yang, F.; Li, Y. Host−Guest Molecular Interaction Enabled Separation of Large-Diameter Semiconducting Single-Walled Carbon Nanotubes. *J. Am. Chem. Soc.* **2021**, *143*, 10120−10130.
(38) Hwang, K.; Lim, D.-H.; Lee, M.-H.; Kim, Y.-J.; Kim, Y.; Yang, D.; Kim, Y.; Kim, D.-Y. Engineering the Structural Topology of Pyrene-Based Conjugated Polymers for the Selective Sorting of Semiconducting Single-Walled Carbon Nanotubes. *Macromolecules* **2021**, *54*, 6061−6072.
(39) Podlesny, B.; Shiraki, T.; Janas, D. One-step Sorting of Single-walled Carbon Nanotubes using Aqueous Two-phase Extraction in the Presence of Basic Salts. *Sci. Rep.* **2020**, *10*, No. 9250.
(40) Yoo, S.; Yi, W.; Khalid, A.; Si, J.; Hou, X. Temperature-dependent Oxidation of Carbon Nanotubes for Metal/Semiconductor Separation. *Chem. Lett.* **2020**, *49*, 1154−1158.
(41) Luo, Y.; Maimaiti, Y.; Maimaitiyiming, X.; Xie, C.; Pei, T. Sorting and Decoration of Semiconducting Single-walled Carbon Nanotubes via the Quaternization Reaction. *RSC Adv.* **2021**, *11*, 2898.
(42) Ju, S. Y.; Abanulo, D. C.; Badalucco, C. A.; Gascón, J. A.; Papadimitrakopoulos, F. Handedness Enantioselection of Carbon Nanotubes Using Helical Assemblies of Flavin Mononucleotide. *J. Am. Chem. Soc.* **2012**, *134*, 13196−13199.
(43) Wei, X.; Tanaka, T.; Hirakawa, T.; Yomogida, Y.; Kataura, H. Determination of Enantiomeric Purity of Single-Wall Carbon Nanotubes Using Flavin Mononucleotide. *J. Am. Chem. Soc.* **2017**, *139*, 16068−16071.
(44) Akazaki, K.; Toshimitsu, F.; Ozawa, H.; Fujigaya, T.; Nakashima, N. Recognition and One-pot Extraction of Right- and Left-handed Semiconducting Single-Walled Carbon Nanotube Enantiomers Using Fluorene-Binaphthol Chiral Copolymers. *J. Am. Chem. Soc.* **2012**, *134*, 12700−12707.
(45) Ao, G.; Streit, J. K.; Fagan, J. A.; Zheng, M. Differentiating Left- and Right-Handed Carbon Nanotubes by DNA. *J. Am. Chem. Soc.* **2016**, *138*, 16677−16685.
(46) Shankar, A.; Zheng, M.; Jagota, A. Energetic Basis of Single-Wall Carbon Nanotube Enantiomer Recognition by Single-Stranded DNA. *J. Phys. Chem. C* **2017**, *121*, 17479−17487.
(47) Wei, X.; Tanaka, T.; Yomogida, Y.; Sato, N.; Saito, R.; Kataura, H. Experimental Determination of Excitonic Band Structures of Single-walled Carbon Nanotubes using Circular Dichroism Spectra. *Nat. Commun.* **2016**, *7*, 12899.
(48) Wei, X.; Tanaka, T.; Hirakawa, T.; Tsuzuki, M.; Wang, G.; Yomogida, Y.; Hirano, A.; Kataura, H. High-yield and High-throughput Single-chirality Enantiomer Separation of Single-wall Carbon Nanotubes. *Carbon* **2018**, *132*, 1−7.
(49) Li, H.; Gordeev, G.; Garrity, O.; Peyyety, N. A.; Selvasundaram, P. B.; Dehm, S.; Krupke, R.; Cambré, S.; Wenseleers, W.; Reich, S.; Zheng, M.; Fagan, J. A.; Flavel, B. S. Separation of Specific Single-Enantiomer Single-Wall Carbon Nanotubes in the Large Diameter Regime. *ACS Nano* **2020**, *14*, 948−963.
(50) Xu, L.; Valášek, M.; Hennrich, F.; Sedghamiz, E.; P-Amion, M.; Häussinger, D.; Wenzel, W.; Kappes, M. M.; Mayor, M. Enantiomeric Separation of Semiconducting Single-Walled Carbon Nanotubes by Acid Cleavable Chiral Polyfluorene. *ACS Nano* **2021**, *15*, 4699−4709.
(51) Wei, X.; Tanaka, T.; Li, S.; Tsuzuki, M.; Wang, G.; Yao, Z.; Li, L.; Yomogida, Y.; Hirano, A.; Liu, H.; Kataura, H. Photoluminescence Quantum Yield of Single-Wall Carbon Nanotubes Corrected for the Photon Reabsorption Effect. *Nano Lett.* **2020**, *20*, 410−417.
(52) Nish, A.; Hwang, J.-Y.; Doig, J.; Nicholas, R. J. Highly selective dispersion of single-walled carbon nanotubes using aromatic polymers. *Nat. Nanotechnol.* **2007**, *2*, 640−646.
(53) Staykov, A.; Ooishi, Y.; Ishihara, T. Immobilizing Metal Nanoparticles on Single Wall Nanotubes. Effect of Surface Curvature. *J. Phys. Chem. C* **2014**, *118*, 8907−8916.
(54) Lin, C. S.; Zhang, R. Q.; Niehaus, T. A.; Frauenheim, T. Geometric and Electronic Structures of Carbon Nanotubes Adsorbed with Flavin Adenine Dinucleotide: A Theoretical Study. *J. Phys. Chem. C* **2007**, *111*, 4069−4073.
(55) Gotovac, S.; Honda, H.; Hattori, Y.; Takahashi, K.; Kanoh, H.; Kaneko, K. Effect of Nanoscale Curvature of Single-Walled Carbon Nanotubes on Adsorption of Polycyclic Aromatic Hydrocarbons. *Nano Lett.* **2007**, *7*, 583−587.

https://doi.org/10.1021/acs.jpcc.2c00959
J. Phys. Chem. C XXXX, XXX, XXX−XXX